Journal of Engineering Physics and Thermophysics, Vol. 70, No. 4, 1997

NUMERICAL MODELING OF ELECTRIC ARCS

J. A. Bakken[a], L. Gu[a], H. L. Larsen[a], and V. G. Sevastyanenko[b]

UDC 537.523.5

Thermal plasmas generated by electric arc discharges between various types of electrodes or by plasmatrons have many well-established – and numerous potential – applications in extractive metallurgy, materials processing and high temperature chemistry. The current is from below 100 A in welding arcs to above 100 kA in electric arc furnaces (EAF) for steel-making and submerged arc furnaces (SAF) for production of silicon alloys. AC as well as DC is used. To improve process understanding and equipment design a number of simulation models have been developed, reaching higher levels of sophistication as more computer capacity has become available. This report reviews the state-of-the-art of arc simulation and discusses some important problems and challenges for future modelling work – in particular on high currents and AC operation. The perspective is the metallurgical and chemical engineers' demand for practical simulation models – not the physicist's very stringent approach.

Introduction. Arc discharges have found widespread applications in various fields of high temperature processing. There is an ever increasing demand for more energy efficient processes and reactors, better process control and lower maintenance costs of electrodes and furnace linings. For this reason, numerical simulation of fluid flow and heat and mass transfer in arcs will probably be more and more important. The aim of this report is to review briefly the development of arc modelling, and to discuss some of the problems that need to be studied more carefully in future modelling work on thermal plasmas. High currents and AC arcs are emphasized.

2. Channel Arc Models. The channel arc models (CAM) do not require the solution of a set of coupled non-linear partial differential equations, and can be run on any PC. In the primitive CAM description the arc coloumn is assumed to be a uniform *cylinder* exept for a short cathode contraction. Here the Lorentz force $\mathbf{j} \times \mathbf{B}$ generates a plasma jet, which converts energy from the arc towards the anode.

For a given current I and arc length L the uniform channel temperature T and radius R are the two main quantities to be determined. The equations to be satisfied are the *integral energy balance* of the arc and a second equation provided by *Steenbeck's energy minimum principle* [1]:

$$P_{el} = \Sigma \text{ heat losses}, \quad \frac{\partial P_{el}}{\partial R}\, dR + \frac{\partial P_{el}}{\partial T}\, dT = 0 \tag{1}$$

Channel models might be useful for estimating current-voltage characteristics of DC as well as AC arcs considered as non-linear elements in the electric circuits of EAFs and SAFs.

3. Models Based on Differential Conservation Equations. The channel arc models are based on *integral balances* for mass, momentum and energy. They can give no information about the "inner structure" of the arc. To obtain more detailed information, e.g., the temperature and velocity distributions, the arc and its nearest surroundings must be divided into a large number of small computational cells. The *mass, x-, y-* and *z-momentum, energy and electric charge* balances for each of these cells must be satisfied. In other words: a system of conservation (or transport) equations in the form of a set of non-linear and nasty *coupled partial differential equations* must be solved with appropriate boundary conditions. The 3D time-dependent conservation equations can be written in Cartesian tensor form.

[a]Dept. of Metallurgy, The Norwegian Institute of Technology, Norway; [b]Dept. of Technical Physics, Belarusian Polytechnic Academy, Minsk, Belarus. Published in Inzhenerno-Fizicheskii Zhurnal, Vol. 70, No. 4, pp. 532-544, July-August 1997. Original article submitted October 10, 1995.

 1062-0125/97/7004-0530$18.00

The continuity equation

$$\frac{\partial \rho}{\partial t} + \frac{\partial (\rho v_i)}{\partial x_i} = 0 \tag{2}$$

i is a subscript that denotes the three space coordinates and v_i denotes the three velocity componets.

The momentum equations

$$\frac{\partial (\rho v_i)}{\partial t} + \frac{\partial (\rho v_i v_j)}{\partial x_j} = -\frac{\partial p}{\partial x_i} + \frac{\partial \tau_{ij}}{\partial x_j} + F_i \tag{3}$$

F_i is the i-components of the body forces, e.g., the Lorentz force. The stress tensor is given by

$$\tau_{ij} = \mu_{\text{eff}} \left(\frac{\partial v_i}{\partial x_j} + \frac{\partial v_j}{\partial x_i} \right) - \frac{2}{3} \mu_{\text{eff}} \delta_{ij} \nabla \cdot \mathbf{v} \tag{4}$$

μ_{eff} is the effective viscosity: $\mu_{\text{eff}} = \mu + \mu_t$, where μ_t is the turbulent viscosity. To compute μ_t a turbulence model must be used, e.g. the k-ε-model – see Sect. 8.

The energy equation

$$\frac{\partial (\rho h)}{\partial t} + \frac{\partial (\rho v_j h)}{\partial x_j} = \frac{\partial}{\partial x_j} \left(\frac{k_{\text{eff}}}{c_p} \frac{\partial h}{\partial x_j} \right) + S_h \tag{5}$$

K_{eff} represents the effective thermal conductivity:

$$\frac{k_{\text{eff}}}{c_p} = \frac{k}{c_p} + \frac{\mu_t}{\text{Pr}_t} \tag{6}$$

where Pr_t is the turbulent Prandtl number and k the molecular thermal conductivity. S_h is a general source term, which includes ohmic heating, radiation, etc. – see Sect. 7.3.

In addition, conservation (diffusion) equations for *chemical species* might be included.

3.1. The Prescribed Current Distribution Approximation. To reduce the numerical complexity, various simplifying assumptions were made in earlier works on arc modelling. For free-burning axisymmetric DC arcs in argon a prescribed current density distribution $j_z(r, z)$ was first used by Ramakrishnan et al. [2]. Analytic expressions are given for the *parabolic* distribution $j_z(r)$ and the expanding arc radius $R(z)$:

$$j_z(r, z) = \frac{2I}{\pi R^2} \left(1 - \frac{r^2}{R^2} \right), \quad R(z) = R_{\text{ca}} \left(1 - C \frac{z^{1/2}}{R_{\text{ca}}^{1/2}} \right) \tag{7}$$

where R_{ca} is the assumed cathode spot radius (e.g. determined by the Richardson–Dushman formula) and C is an empiric or adjustable "arc expansion factor." The azimuthal magnetic field B_θ and the radial and axial components of *the Lorentz force* $\mathbf{j} \times \mathbf{B}$ are then obtained analytically from (7):

$$B_\theta(r, z) = \frac{\mu_0 I}{2\pi R^2} r \left(2 - \frac{r^2}{R^2} \right), \quad F_r = j_z B_\theta, \quad F_z = j_r B_\theta \tag{8}$$

$$j_r(r, z) = \frac{I}{\pi R^3} C \frac{R_{\text{ca}}^{1/2}}{z^{1/2}} r \left(1 - \frac{r^2}{R^2} \right) \tag{9}$$

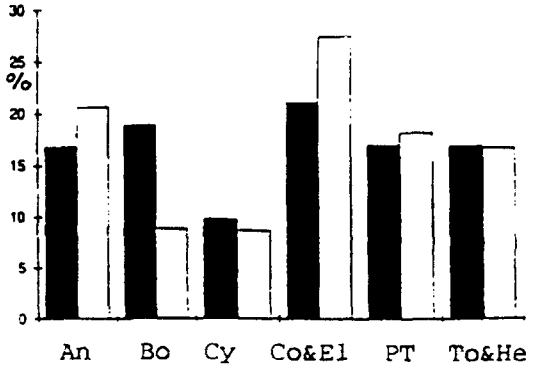

Efficiency	Computed	Measured
Torches	73%	76%
Reactor chamber	61%	53%
Overall	45%	41%

Fig. 1. Heat distribution in the triple-torch calorimeter– computed and measured values . An = anode, Pt = plasma torch, To&He = off-gas, etc.

Fig. 2. Thermal efficiencies by remelting of silicon metal fines – computed and measured values.

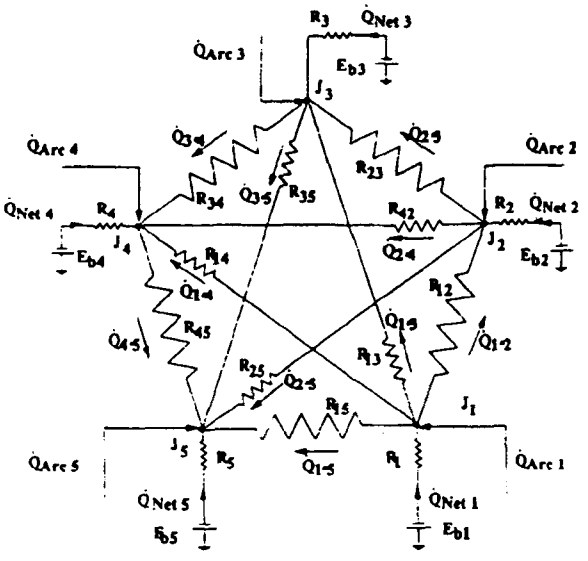

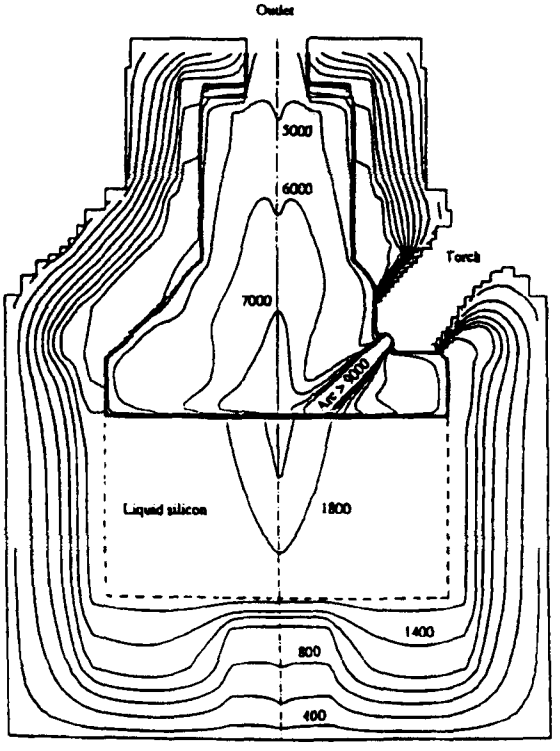

Fig. 3. Analog electric circuit for wall-to-wall radiation.

Fig. 4. Temperature distribution in triple-torch plasma reactor

With this rather dubious model the current density distribution does not depend on the electric conductivity and hence the temperature. This means that the electric and magnetic fields are *decoupled* from the temperature distribution and the flow field!

The prescribed current approximation gives an inaccurate arc description and tends to overestimate the ohmic heating j^2/σ in the arc fringes and near the cathode. It may still be useful, however, for computing the convective and radiative *heat flux distribution* on the surrounding reactor surfaces – i.e., "long-distance effects" – and to predict the *thermal efficiencies* of the plasma torches and the reactor chamber as shown for the 3D case of a plasma reactor with three tilted transferred arcs [3] – see Figs. 1 and 2.

The thermally isolated lining is included in the computational domain, and the important *wall-to-wall radiation* is taken into account employing the analog electric circuit of Fig. 3. As shown in Fig. 4 the wall temperatures are calculated rather than given as boundary conditions.

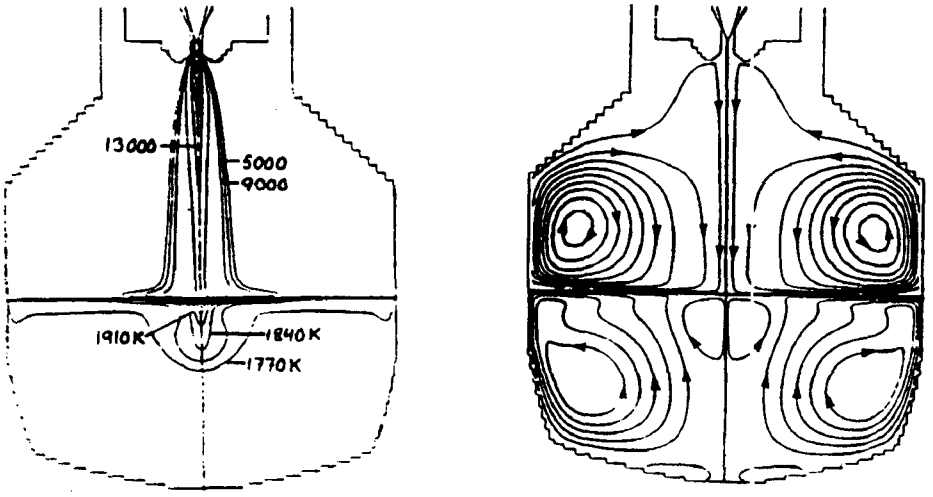

Fig. 5. Temperature distribution in the gas phase and the anodic metal pool.

Fig. 6. Stream lines in the gas phase (V_{max} = 900 m/sec) and the metal pool

3.2. Computed Current and Magnetic Field Distributions. The shortcomings of the prescribed current approximation made it desirable to *calculate the current distribution* by solving Maxwell's equations (or the current continuity equation) and Ohm's law together with the conservation equations for mass, momentum and energy. Thus the strong *coupling* between the temperature and velocity fields and the current distribution through the Lorentz force and the temperature dependent conductivity is accounted for.

The j and B fields can be computed in different ways depending on the most convenient type of boundary conditions to be used. One can start by computing the potential distribution $\phi(r,D,z)$, then j by derivation using Ohm's law, and finally B by integration of Ampere's law:

$$\frac{1}{r}\frac{\partial}{\partial r}\left(\sigma r\frac{\partial\varphi}{\partial r}\right)+\frac{\partial}{\partial z}\left(\sigma\frac{\partial\varphi}{\partial z}\right)=0\,,\quad j_r=-\sigma\frac{\partial\varphi}{\partial r}\,,\quad j_z=-\sigma\frac{\partial\varphi}{\partial z}\,,\quad \frac{1}{r}\frac{\partial\,(rB_\theta)}{\partial r}=\mu_0 j_z \tag{10}$$

Alternatively, one can start by solving *the transport equation* for B and then get j by derivation employing Ampere's law. The last method is used in the AC model presented in Sect. 7 and seems advantageous compared to the vector potential approach when induction effects must be taken into account.

4. Anodic Metal Pools. Fluid flow and heat transfer in anodic metal pools are important in many applications, e.g. plasma arc welding and tundish heating as well as DC EAP furnaces for steelmaking. The circulating flow in the metal pool is driven by a combination of *Lorentz forces* due to the passage of the arc current, surface shear forces caused by the impinging *cathode jet*, shear forces due to *surface tension gradients* (Marangoni effect) and *buoyancy*.

A *two-step iterative* procedure was used by Gu et al. [4, 5] to calculate the velocity and temperature fields in the metal pool. The conservation equations for the two computational domains – the gas phase and the liquid metal phase are solved separately. In both domains the k-ε turbulence model is used. The continuity of electric current, momentum and heat transport across the gas–metal interface is expressed as boundary conditions for the two domains. The temperature distribution and the stream lines shown in Figs. 5 and 6 refer to a 600 A, 183 mm long, 30 Nl *argon*/min transferred arc with an anodic *silicon* metal pool. Two circulation zones are seen in the pool: a small electromagnetic force dominated zone near the arc foot and a large zone dominated by jet momentum and Marangoni forces. Buoyancy forces are negligible in this case.

5. Effect of Metal Vapours on Arc Behaviour. Discrepancies between computed and measured arc voltages could in some cases be attributed to infiltration of small amounts pf metal vapour originating from the electrode surfaces – particularly when a *metal pool* is serving as anode for a transferred arc, and if the liquid metal is contaminated with low-boiling and easily ionizable elements as Ca and Al. These elements tend to increase the electric conductivity and thus *reduce* the arc voltage. At the same time, however, the radiation losses would tend

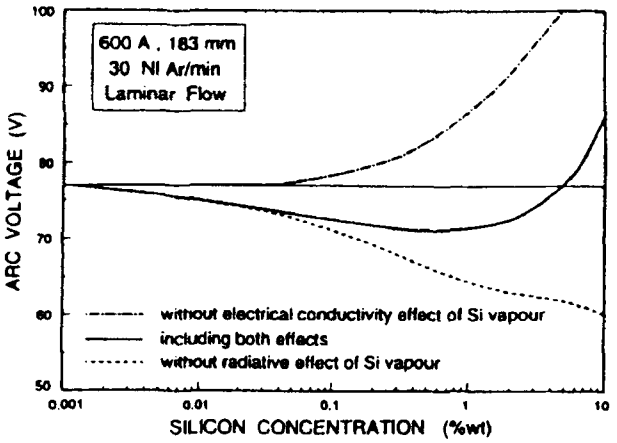

Fig. 7. Computed voltage of a transferred arc in *argon* infiltrated by *silicon* vapour vs conc. [wt-% Si]: --- without el.conductivity effect; – including both effects; ... without radiative effect of Si.

to increase. For this reason the voltage required to sustain the arc would become *higher*. The first effect dominates at *low* concentrations and the second at *higher* vapour concentrations. This is clearly seen in Fig. 7, which refers to simulations on a 600 A, 183 mm long and 30 Nl *argon*/min transferred arc burning against an anodic *silicon* metal pool. Here the influence of an assumed *uniform* vapour distribution has been evaluated without solving the conservation equation for the metal vapour, i.e., without considering the diffusion problem.

6. Diffusion in Arc. *6.1. The Quasi-Binary Diffusion Coefficient.* For *binary* plasmas (e.g. Ar-Cu) the ordinary binary diffusion coefficients of the *neutral* atoms have often been used to describe mass transport. This simplifying assumption is hardly justified in arc plasma where diffusion of ions are dominant. The concept of quasi-binary diffusion coefficients (QBDCs) was introduced by Gu et al. [4, 5] to study *silicon infiltrated argon arcs.* As an approximation under LTE conditions and due to ambipolar diffusion it is assumed that the neutral atoms (Si) move at the same speed as the ions (Si^+, Si^{2+}...) and their accompanying electrons. From the fundamental Stefan–Maxwell diffusion equations

$$\nabla X_i = \sum \frac{1}{CD_{ij}} (X_i N_j - X_j N_i) = \sum \frac{X_i X_j}{D_{ij}} (\mathbf{v}_j - \mathbf{v}_i) , \quad i = 1, 2, ..., n \tag{11}$$

the *molar flux* expression for the Si atoms and ions (species *group S*) can be deduced:

$$\mathbf{N}_S = - CD_{AS} \nabla X_S + X_S (\mathbf{N}_A + \mathbf{N}_S) \tag{12}$$

where *the quasi-binary diffusion coefficient* $D_{AS} = D_{SA}$ is expressed by the molar fractions x_i of all species i and the ordinary binary diffusion coefficients D_{ij} of all pairs ij of species:

$$D_{AS} = \frac{(X_{Ar} + 2X_{Ar^+} + 3X_{Ar^{2+}} + \cdots)(X_{Si} + 2X_{Si^+} + 3X_{Si^{2+}} + \cdots)}{X_{Ar}\left(\frac{X_{Si}}{D_{ArSi}} + \frac{X_{Si^+}}{D_{ArSi^+}} + \frac{X_{Si^{2+}}}{D_{ArSi^{2+}}} + \cdots\right) + X_{Ar^+}\left(\frac{X_{Si}}{D_{Ar^+Si}} + \frac{X_{Si^+}}{D_{Ar^+Si^+}} + \frac{X_{Si^{2+}}}{D_{Ar^+Si^{2+}}} + \cdots\right) + \cdots} \tag{13}$$

D_{AS} thus depends on the local *element ratio* Ar:Si and the local temperature. In Eqs. (3)-(4) the concentrations were expressed as *mole* fractions whereas *mass* fractions are far more convenient in arc models. The required transformation to mass based equations is a purely mathematical operation.

6.2. The Quasi-Ternary Diffusion Coefficients. Highly complex *ternary* plasmas, i.e. plasmas composed of three *elements*, are for example found in the industrial submerged arc furnace for production of silicon metal. In the cavities or craters, where the AC arcs (~ 100 kA) burn, SiO and CO are the dominant molecular species. Thus plasmas composed of Si, O and C must be considered if one wants to model these arcs. The QBDC concept might

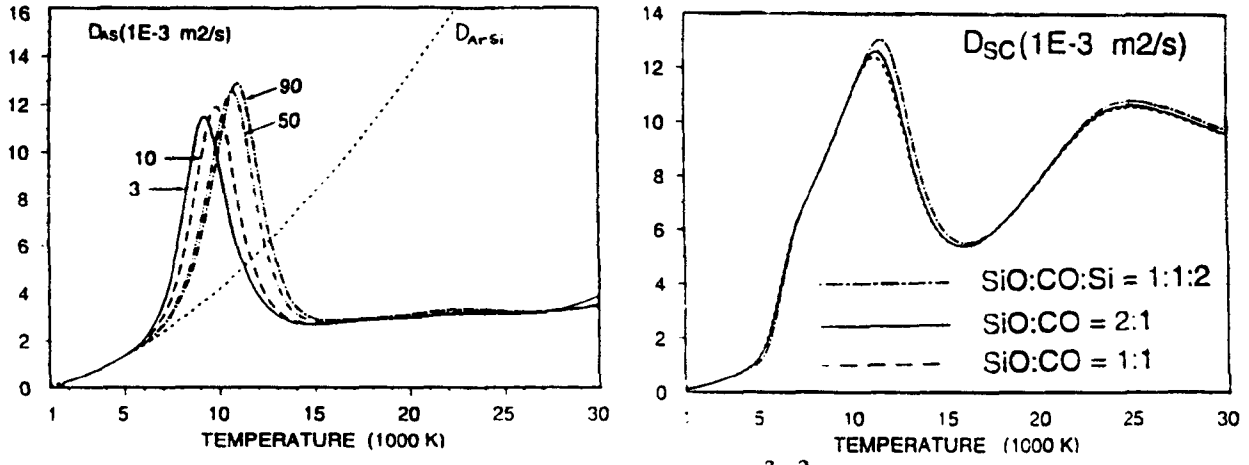

Fig. 8. Quasi-binary diffusion coefficient D_{AS} [10^{-3}m^2/sec] of Ar-Si mixtures compared to the ordinary binary atom-atom coefficient D_{ArSi} as a function of temperature.

Fig. 9. Quasi-binary diffusion coefficient D_{SC} [10^{-3} m^2/sec] of quasi-ternary Si-O-C plasmamixtures.

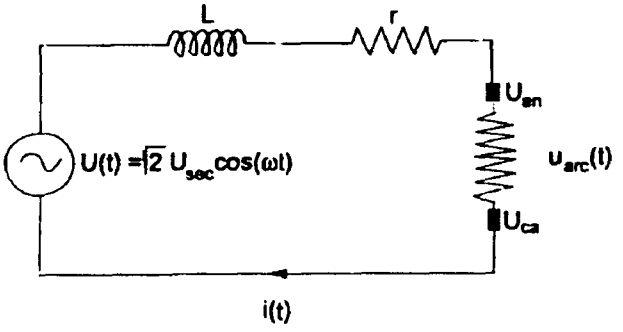

Fig. 10. The electric circuit of an AC electric arc furnace – EAF or SAF.

– with some algebraic effort – be extended to ternary plasmas A-B-C. With W_i denoting *mass fractions*, the flux equations for species *groups* A and B becomes:

$$\begin{aligned} \mathrm{m}_A &= -\rho D_{AA}\nabla \mathrm{W}_A - \rho D_{AC}\nabla \mathrm{W}_C + \mathrm{W}_A\,(\mathrm{m}_A + \mathrm{m}_B + \mathrm{m}_C) + \xi_A \\ \mathrm{m}_B &= -\rho D_{BB}\nabla \mathrm{W}_B - \rho D_{BC}\nabla \mathrm{W}_C + \mathrm{W}_B\,(\mathrm{m}_A + \mathrm{m}_B + \mathrm{m}_C) + \xi_B \end{aligned} \tag{14}$$

where the *four* "multi-component" coefficients D_{AA}, D_{AC}, D_{BB} and D_{BC} are expressed by *three* QBDCs as described above: D_{AB}, D_{BC} and D_{AC}. ξ_A and ξ_B are "electron compensation" terms. Typical examples of the temperature dependence of QBDCs are shown in Figs. 8-9.

7. AC Arc Models. *7.1. The Electric Circuit.* In most high power applications as EAFs and SAPs the power source is a transformer with a high voltage primary winding (typically 100 kV) and a low voltage, high current secondary (typically 100-1000 V, 100 kA). The arc current is *not given* – as is always assumed when modelling DC arcs. What normally is given is *the external electric circuit* consisting of an ideal voltage source U_{sec} representing the transformer secondary, a lumped inductance L and a lumped loss resistance r as indicated in Fig. 10. This circuit can be described by a linear first-order differential equation

$$\sqrt{2}\,U_{sec}\cos(\omega t) = L\frac{di}{dt} = ri + u_{arc}(t) \tag{15}$$

u_{arc} is the calculated arc voltage, which includes the induced voltage due to the time-varying strong magnetic flux through the arc region:

$$u_{arc}(t) = \int_0^H E_z(0, z, t)\, dz - \frac{d}{dt} \int\int_A B_\theta(r, t)\, drdz + U_{an} + U_{ca} \tag{16}$$

U_{an} is the *anodic* and U_{ca} is the *cathodic fall voltage.*

At each time-step an updated u_{arc}-value is inserted in (15), and a new arc current $i(t)$ is obtained by simple integration. The electric circuit equations (15) and (16) can of course be used in combination with any AC arc model, e.g., the two models to be described below.

7.2. AC Channel Arc Model. The CAM concept was successfully applied to alternating current arcs in 1980 by Sakulin [1] and later improved by Pfeifer et al. [2] and Larsen [3]. When simulating AC arcs the basic idea is that the arc at all times tries to approach the state of equilibrium of a hypothetical DC *arc channel* with current equal to the instantaneous AC current. The *time constant* involved is treated as an empiric or adjustable parameter, which probably depends on the current. It is typically 1 millisecond.

7.3. AC Arc Model Based on Differential Conservation Equations. The CAM description is useful if one wants if one wants to simulate an AC arc as a non-linear resistive element in the electric circuit of an arc furnace. Despite its simplicity the channel model is able to predict the main features such as the "hystereses" of the *dynamic* current-voltage characteristics, i.e., *u(t) versus i(t)*, and the Fourier spectra of the current and voltage waveforms. Far more sophisticated mathematical models must be applied to obtain more detailed and accurate information about the time-varying current, temperature and velocity distributions. The problems that have to be dealt with in DC arc modelling are of course also encountered when AC arcs are studied. In addition, several new problems arise – particularly at very high currents. With AC the time-dependent conservation equations for mass, momentum and energy, the Maxwell equations with Ohm's law must be solved for 50 Hz periodically varying distributions of current density, temperature, velocity, etc. For a cylindrically symmetric arc the relevant 2D conservation equations can be written as follows.

Mass:

$$\frac{\partial \rho}{\partial t} + \frac{1}{r}\frac{\partial}{\partial r}(r\rho v_r) + \frac{\partial}{\partial z}(\rho v_z) = 0\,, \tag{17}$$

Radial momentum:

$$\frac{\partial}{\partial t}(\rho v_r) + \frac{1}{r}\frac{\partial}{\partial r}(r\rho v_r v_r) + \frac{\partial}{\partial z}(\rho v_z v_r) =$$

$$= -\frac{\partial p}{\partial r} + \frac{1}{r}\frac{\partial}{\partial r}\left(2r\mu\frac{\partial v_r}{\partial r}\right) + \frac{\partial}{\partial z}\left(\mu\left(\frac{\partial v_r}{\partial z} + \frac{\partial v_z}{\partial r}\right)\right) - \frac{2\mu v_r}{r^2} - j_z B_\theta\,, \tag{18}$$

Axial momentum:

$$\frac{\partial}{\partial t}(\rho v_z) + \frac{1}{r}\frac{\partial}{\partial r}(r\rho v_r v_z) + \frac{\partial}{\partial z}(\rho v_z v_z) =$$

$$= -\frac{\partial p}{\partial z} + \frac{1}{r}\frac{\partial}{\partial r}\left(r\mu\left(\frac{\partial v_r}{\partial z} + \frac{\partial v_z}{\partial r}\right)\right) + \frac{\partial}{\partial z}\left(2\mu\frac{\partial v_z}{\partial z}\right) + j_r B_\theta\,, \tag{19}$$

Energy:

$$\frac{\partial}{\partial t}(r\rho h) + \frac{1}{r}\frac{\partial}{\partial r}(r\rho v_r h) + \frac{\partial}{\partial z}(\rho v_z h) =$$

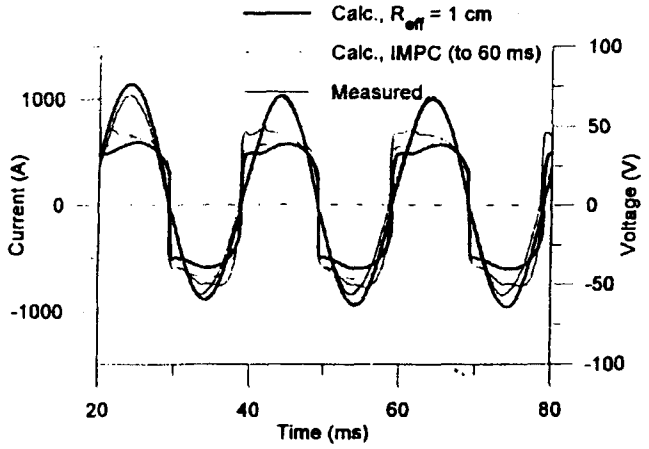

Fig. 11. Computed current and voltage waveforms of a 40 mm AC arc in *argon* at 695 A rms.

$$= \frac{\partial}{\partial r}\left(r\frac{k}{c_p}\frac{\partial h}{\partial r}\right) + \frac{\partial}{\partial z}\left(\frac{k}{c_p}\frac{\partial h}{\partial z}\right) + \frac{j_r^2 + j_z^2}{\sigma} + \frac{5k_B}{2e}\left(\frac{j_r}{c_p}\frac{\partial h}{\partial r} + \frac{j_z}{c_p}\frac{\partial h}{\partial z}\right) - S_{rad} + \frac{Dp}{Dt}, \tag{20}$$

S_{rad} is the radiation term, i.e. the divergence of the radiative heat flux (cf. Sect. 9). The last term takes care of compressibility effects (see Sect. 11). In addition, pressure dependent thermodynamic and transport properties should be used.

The magnetic transport equation:

$$\frac{\partial B_\theta}{\partial t} + \frac{1}{r}\frac{\partial}{\partial r}(rv_r B_\theta) + \frac{\partial}{\partial z}(v_z B_\theta) = \frac{\partial}{\partial r}\left(\Gamma_m \frac{1}{r}\frac{\partial}{\partial r}(rB_\theta)\right) + \frac{\partial}{\partial z}\left(\Gamma_m \frac{\partial B_\theta}{\partial z}\right) \tag{21}$$

$\Gamma_m = 1/(\mu_0\sigma)$ *is the magnetic diffusivity*, which governs the diffusion of the magnetic flux through the arc plasma.

At high currents (10^4–10^3 A) and flow velocities (10^3–10^4 m/sec) the induced electric field $v \times B$ due to the motion of the plasma across the magnetic field lines may not be negligible compared to the applied field. Ohm's law then becomes:

$$j = \sigma(E + v \times B) \tag{22}$$

Even at the low power grid frequency of 50 Hz electromagnetic induction effects or "skin effect" due to $\partial B/\partial t$ – well known from RF induction plasma torches – may be significant in high current AC arcs, where a phase shift will occur between the current in the core and the fringes of the arc. The total instantaneous power obtained by integrating the ohmic heating j^2/σ over the entire arc will then no longer be exactly equal to the product of arc voltage and current.

Both induction effects, $v \times B$ and $\partial B/\partial t$, are included in the magnetic field equation (21).

The simulated current and arc voltage waveforms for a 40 mm long freeburning AC arc in *argon* are shown in Fig. 11, which refers to a laboratory arc operated at an rms current of 695 A. The transformer secondary voltage is 192 V rms and the external circuit inductance is 0.84 mH.

The temperature distributions in the positive and negative half periods are shown in Fig. 12.

8. **Local Thermodynamic Equilibrium.** So far, most arc models have been based on the simplifying assumption of **local thermodynamic equilibrium** (LTE). How serious are *deviations from LTE* in the DC and AC arcs used in metallurgical and chemical applications? It is generally recognized that non-LTE effects are important *near the electrodes and in the arc fringes* – see Fig. 15. With AC, deviations from LTE are to be expected everywhere in the arc when the current passes zero.

A **two-temperature** description of the entire arc would of course be the best way of coping with the LTE problem. There are two obstacles for realizing a two-temperature model: i) A more complicated set of coupled PFEs

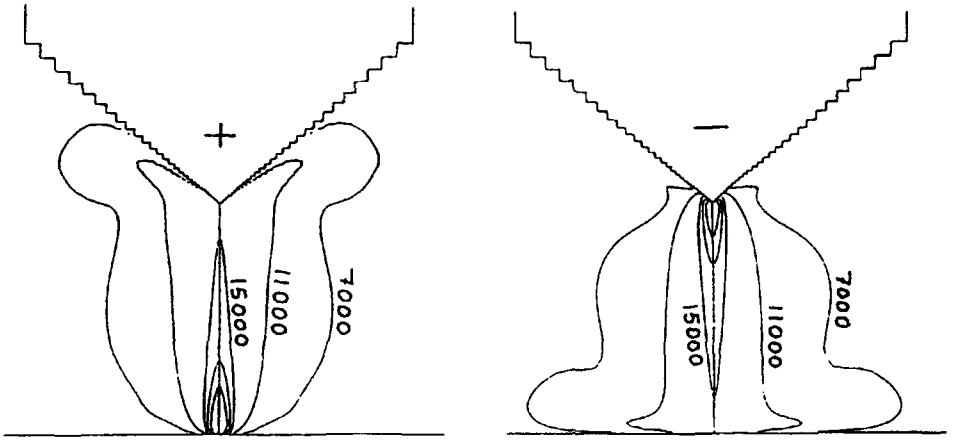

Fig. 12. Momentaneous temperature distribution in the positive (I = +969 A) and negative (I = 881 A) half periods of a 40 mm free-burning AC arc in *argon*, 695 A rms.

must be solved as mass, momentum and energy balances must be formulated separately for the atoms plus ions and for the light electrons. ii) Only a limited amount of thermodynamic data, transport coefficients and radiative properties are presently available for gases other than argon. Two-temperature models have, however, been used for the cathode region (see Sect. 14).

9. Turbulence Modelling. In most numerical modelling work on arcs one has either assumed *laminar* flow or employed the k-ε turbulence model. This is an isotropic, high-Reynolds-number model, which tends to overestimate the turbulent in the high-temperature, high-viscosity core of the arc. Although the *Prandtl mixing length* approach and modified *k-ε* models with *variable "constants"* have been tried by some authors the results so far do not seem satisfactory. None of these models account for the presence of the magnetic field. The magnetic field introduces *anisotropy* and *damping* of the turbulent velocity normal to the field [11]. A modified version of *Reynolds' stress model* for turbulence in liquid metal flows may perhaps offer a better way of simulating turbulence in arcs.

10. Radiation – Optically Thin or With Reabsorption? Most previous arc simulations have been based on the optically thin plasma approximation, which implies that the locally emitted radiation escapes from the plasma without reabsorption. Volumetric radiation densities to be used with this simplified radiation model are obtained by measurements on arcs with similar geometries and currents. A physically more correct description is obtained by calculating the power radiated per unit volume which escapes from an isothermal sphere or cylinder, thus defining an effective radiation radius. This method can only give approximate results.

A considerably more refined and accurate method of modelling radiative heat exchange which elegantly takes reabsorption into account is the integral method of partial characteristics (IMPC) developed by Sevastyanenko [12]. Outside the former USSR, Arnsberg et al. [13] were the first to apply this method to arc modelling, but the IMPC method now seems to be gaining international acceptance. According to the IMPC approach *the intensity* $I_\nu(x, \Omega\omega)$ [W/m^2·sr] at a given "sink" point x in the Ω-direction is calculated as a sum of contributions ΔI from "source" points ξ along the direction Ω:

$$I(x, \Omega\omega) = \int_{\xi=x}^{L} \Delta I(T_\xi, T_x, \xi - x)\, d\xi \tag{23}$$

$$\Delta I(T_\xi, T_x, \xi - x) = \int_0^\infty I_\nu^0(T_\xi)\, k_\nu'(T_\xi) \exp\left[-\int_0^{\xi-x} k_\nu'(T_\eta)\, d\eta\right] d\nu \tag{24}$$

The so-called partial characteristics ΔI [W/m^3·sr] are functions of the source temperatures T_ξ, the sink temperature T_x and the source-sink distance $\xi - x$. k_ν' is *the spectral absorption coefficient*, which must be known or

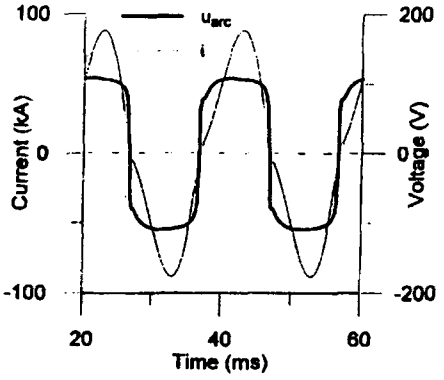

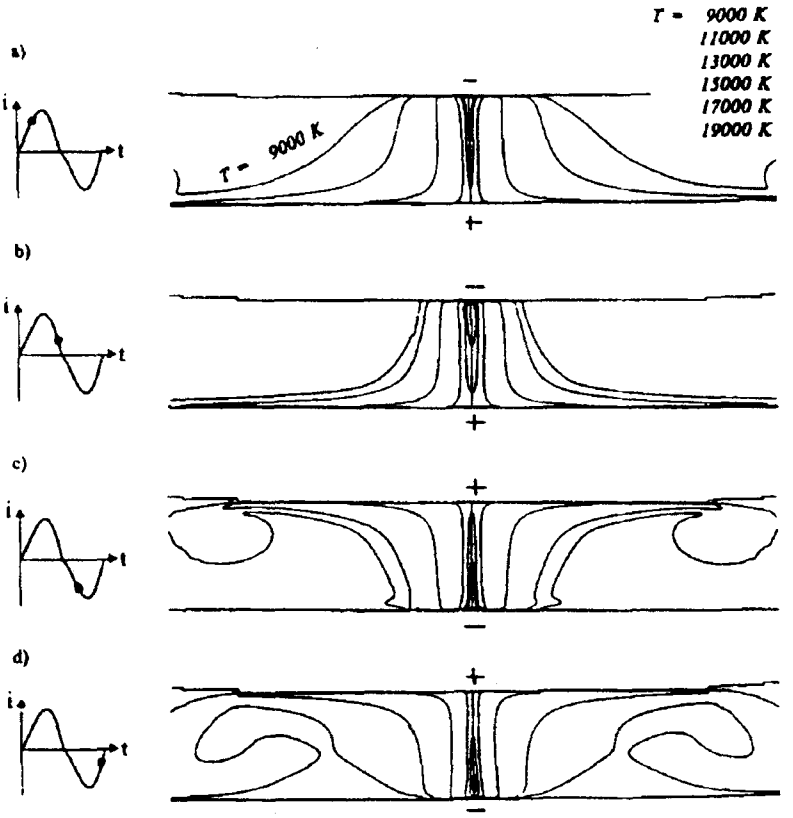

Fig. 13. Computed current and voltage waveforms of an AC arc in a 22 MW SAF. Rms current 77 kA.

Fig. 14. Computed isotherms in an AC arc of a 22 MW SAF at different times during a cycle.

computed from atomic data. ΔI and I *are total* quantities which result from integrating over all spectral frequencies ν in (7). The upper limit L in (6) is the distance in the Ω-direction from x to the boundary of the radiating volume.

The radiation flux density $\dot{q}_{rad}$ [W/m^2] obtained by integrating the intensity over all solid angles:

$$\dot{q}_{rad} = \int_{4\pi} \int \Omega \, I \, d\omega \tag{25}$$

The radiation source term in the energy conservation equation is the *divergence* of $\dot{q}_{rad}$ [W/m^3], which is also calculated using partial characteristics:

$$S_{rad} = \int_{4\pi} \int \nabla \cdot (\Omega \, I) \, d\omega \tag{26}$$

Based on linearized – or higher order – temperature distributions over $\xi - x$, ΔI-values for any desired combination of source and sink temperatures (T_ξ, T_x) and source-sink distances $\xi - x$ can be precalculated, and easy-to-use tables for different gases or gas mixtures established [14, 15].

In industrial high current applications the prediction of radiative heat transfer to surrounding reactor surfaces is important from the point of view of *efficient heat transfer* to the reaction zone as well as minimizing *wear* of the refractory lining, and to identify *highly exposed* wall sections which need extra cooling. The IMPC approach lends itself easily to calculation of radiation heat transfer to solid or liquid surfaces surrounding the arc.

A detailed account of the IMPC method and possible improvements of its accuracy will be given by Prof. Sevastyanenko at this seminar.

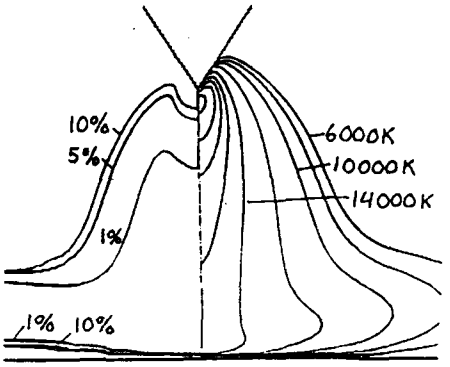

Fig. 15. Deviations from LTE: distribution of the critical ratio $(T_e - T_h)/T_h$ (left) and the plasma temperature T_h (right) in a 200 A. 10 mm long free-burning DC arc in *argon*.

11. Compressibility Effects. At the high currents found in EAPs (10^4–10^3 A) the Lorentz forces obviously generate high velocities (10^3–10^4 m/sec), which may not be negligible compared to *the local velocity of sound c*. If the condition $v^2 << c^2$ is not fulfilled, in practice if *the Mach number* $v/c > 0.3$, one should take into account the effect of **local pressure variations** on the mass density as well as the thermodynamic, transport and radiation properties. In arc modelling these quantities have usually been taken at the *ambient* pressure (normally 1 bar). It is not satisfactory to consider only the density variations according to the ideal gas law.

12. Depression of Liquid Metal Electrode Surfaces at High Currents. In published numerical models of transferred and free-burning arcs the anode surface is assumed to be *flat* even in the case of liquid anodes. It is well known from electric arc furnaces for steelmaking that the arc exerts strong forces – mainly of electromagnetic origin – on the surface of the steel bath around the arc root, thus causing a depression of considerable depth. According to Bowman [16], the depression is typically 20 cm deep at 40 kA rms provided that the arc is stable. Instabilities tend to decrease the depression. In the case of a high current DC arc burning against an anodic metal pool, the depression would be expected to be even deeper. In addition to creating a depression, the $\mathbf{j} \times \mathbf{B}$ forces set up in the steel bath by the arc current also generates vigourous motion or stirring – cf. Sect. 4.

The depression effect most probably influences the arc voltage and energy transfer characteristics and should be seriously considered in modelling work on industrial high current arcs.

13. Arc Instabilities. Arc instability is a well known and unpopular phenomenon for all who have tried to do measurements on arc discharges, or are familar with industrial high current arcs. The instabilities cause the arc roots to *move irregularly* around on the electrode surfaces, or to make the arc channel *bend* or *twist* [16], or even make it *split up* in several sub-channels with individual electrode spots. This problem is more serious with free-burning arcs than with nozzle-stabilized transferred arcs, and AC arcs tend to be less stable than DC arcs. In some industrial applications arc instabilities are advantageous because they reduce the time-averaged heat flux density on the electrode and the metal pool surface, thus lowering electrode wear and unwanted evaporation of metal. From the academic point of view arc instability is a nuisance, as it might ruin our attempts to compare numerical modelling results with measurements.

In future modelling work various modes of perturbations – with respect to the state of equilibrium – should be imposed on the current and temperature distributions. By calculating the resulting time-dependent behaviour of the arc it should be possible to determine whether a particular perturbation will decay, oscillate or grow with time. Stability analysis is obviously a formidable task which will require a full 3D time-dependent description even in the ideal case of a DC arc in a cylindrically symmetric system. As an example, the helical type of instabilities in a cascade arc are studied by Ragaller et al. [17].

Whether a particular arc can *exist* or not depends critically on the external electric circuit as stated by the well-known *Kaufmann stability criterion*, which however is insufficient to predict instabilities as described above. Another challenge in the field of arc modelling is the *co-existence of multiple arcs*, which are observed under certain conditions.

14. The Cathode Problem. The cathodic current distribution has traditionally been given as a boundary condition expressed in a numerically amenable analytic form, e.g., by an exponential or parabolic equation. With tungsten or graphite cathodes the size of the current emitting spot for a given arc current is usually obtained from the Richardson–Dushman formula for *the thermionic saturation current.* It is assumed that 100% of the arc current is emitted thermionically at a reasonable cathode surface temperature (typically 3500–4000 K for a thoriated W-cathode). Alternatively, the cathode spot size is deduced from optical observations of the arc. These approaches are not satisfactory – particularly if one wants to simulate DC and AC arcs with currents above some kA.

The space charge and the associated cathode fall voltage represent a problem which must be addressed rather than relying on more or less experimentally confirmed guesstimates. To improve the model of the cathode region, *the near-cathode layer* as well as *the solid cathode tip* could in principle be incorporated directly in the over-all computational domain. This approach would of course require an extremely fine numerical grid and very long computation times.

Alternatively, the cathode layer can be included in the arc model as a gaseous sub-domain, which could be one-dimensional due to its very small thickness. The cathode body can be treated as a 2D solid sub-domain. These two sub-domains must then be coupled together, and to the arc plasma main-domain by suitable interphase boundary conditions. To complete the model, deviations from LTE in the layer sub-domain should obviously be accounted for by employing a *two-temperature description.* The *electron* and *ion* current continuity equations together with the *electron* and *heavy* particle energy equations must be solved for the cathode layer. The ion-electron recombination rate is important in this context. The global mass and momentum equations are, however, not necessary in a 1D treatment. In principle, one would then determine the electric field and thus the current distribution as well as the charge density and the cathode fall voltage. In such models the cathode temperature is not predefined, but will emerge as an integral part of the solution for the solid subdomain. If the computed total current density becomes higher than the *saturation* value given by the Richardson–Dushman thermionic emission formula, the excess current must be carried by *positive ions.* These will of course effectively heat the cathode. The temperature of the cathode will give useful information about the maximum current carrying capacity of different electrode materials.

The problem of electron emission from *liquid metals* should be mentioned. In ordinary 3-phase AC furnaces for steelmaking the arcs burn between graphite or Soderberg electrodes and the pool of liquid steel, which acts as a cathode in the negative half periods.

Following the pioneering work of Hsu & Pfender (1983) [18], more and more sophisticated models of the cathode region have been developed [19-24]. Some works also include computations of the temperature distribution in the cathode body.

An entirely different approach was recently proposed by Benilov & Marotta [25, 26]. A simple energy balance is used for the near-cathode layer:

$$j_e\,(U_{ca} - 5kT_e/2e) = j_i\,(U_i + 5kT_e/2e) \tag{27}$$

U_{ca} is the cathode fall voltage, U_i the ionization potential, ϕ the work function and T_e the electron temperature evaluated at the edge of the cathode layer.

From (27) and the R-D formula the electron current j_e and the ion current j_i from the arc plasma to the cathode are calculated as functions of the cathode temperature T_{ca} *for different values of* U_{ca}. The associated *net heat flux density,* which must be conducted into the cathode body, is given by:

$$\dot{q}_{ca} = j_i\,(U_{ca} + U_i - \varphi) - j_e\varphi \tag{28}$$

Whereas the electron emission current j_e increases monotonically with T_{ca}, j_i cannot exceed *the ion saturation current* $j_{i\,sat}$ from the arc plasma. The evaluation of $i_{i\,sat}$ is a crucial step in Benilov's theory. The result is that the $\dot{q}_{ca}(T_{ca})$-function has a sharp maximum and drops off rapidly for lower and higher temperatures T_{ca}. By employing the concept of "non-linear heat structures" the heat conduction problem in the cathode body can be solved with respect to the spot and the total heat flux to the cathode. The total spot current – i.e., the arc current

I corresponding to the chosen U_{ca}-value – is then found by integrating (28). Thus the current-voltage characteristics U_{ca} *versus* I of the cathode region is obtained.

Further development work is needed before this interesting cathode model can be put to practical use in modelling of high current DC and AC arcs.

15. Conclusion. This report reviews some important aspects of arc modelling and points out some problems that need to be looked into in order to improve the reliability of numerical models for DC and AC arcs and extend their applicability to high current levels above 10^3 A. From the above discussion a relatively comprehensive and sophisticated numerical model emerges. With the computers available today the computational time required is usually not a limiting factor in modelling work, but rather our own capacity to write all the algorithms, handle the complex computer code structures and – last but not least – check that the code works properly. This means that the code must be applied to a wide selection of well-designed and verifiable test cases. The work involved in testing and verification should not be underestimated.

With industrial applications in mind the ability of the model to predict the current-voltage characteristics and the distribution of convective and radiative heat on the reactor surfaces should be emphasized.

Acknowledgements. Thanks are due to former Ph. D. and M. Sc. students at The Norwegian Institute of Technology (NTH): Ms. N. J. Holt, Mr. A. E. Arntsberg, Ms. R. Jensen and Mr. A. Hildal, and to our colleague at SINTEF: Mr. R. Jensen. They all participated in the experimental and theoretical plasma research at NTH with great enthusiasm and perseverance.

The work was supported by The Research Association of The Norwegian Ferroalloys Industry (FFF) and The Royal Norwegian Research Council (NFR).

REFERENCES

1. M. Sakulin, Fachberichte Hüttenpraxis Met.verarbeittung, **20**, No. 3 (1982).
2. H. Pfeifer, F. H. Fett, and H. J. Bebber, Elektrowärme int., **3**, B124-B130 (1989).
3. H. L. Larsen, Channel model for AC electric arc, SINTEF, Trondheim, Norway, Report STF34 A931113 (1993).
4. S. Ramakrishnan, A. D. Stokes, and J. J. Lowke, J. Phys. D: Appl. Phys., **11**, 2267-2280 (1978).
5. N. J. Holt, J. A. Bakken, and R. Jensen, ISPC-10, Bochum, Germany (1991).
6. L. Gu, Transport phenomena in silicon vapour infiltrated argon arcs and anodic metal pools, Ph. D., Thesis, Dept. of Metallurgy, The Norwegian Institute of Technology, Trondheim, Norway (1993).
7. L. Gu and J. A. Bakken, Mass, Heat and Momentum Transfer at the Plasma-Metal Pool Interface in a Plasma Arc Reactor, Int. Sem. Heat and Mass Transfer under Plasma Conditions, Cesme, Turkey (1994).
8. L. Gu, Thermodynamic and Transport Properties of and Diffusion in (Ar-)Si-O-C Plasmas, SINTEF, Trondheim, Norway, Report STF34 A94546 (1994).
9. H. J. Larsen, L. Gu, and J. A. Bakken, A Numerical Model for the Arc in the Silicon Metal Furnace, INFACON 7, Trondheim, Norway (1995).
10. H. L. Larsen, A. Hildal, V. G. Sevastyanenko, and J. A. Bakken, Numerical Modelling of AC Electric Arcs, ISPC-12, Minneapolis, USA (1995).
11. S. T. Johansen and L. Gu, A Reynolds stress turbulence model for fluid flow and enthalpy dispersion in strong external magnetic fields. Int. Symp. El.magn. proc. Mat. ISU, Nagoya (1994).
12. V. G. Sevastyanenko and R. I. Soloukhin (ed.), Handbook of Radiative Heat Transfer in High-Temperature Cases, R. Goulard (Eng. ed.), Hemisphere Publ. Corp./Springer-Verlag (1987).
13. A. E. Arntsberg, L. Gu, and J. A. Bakken, J. High Temp. Chem. Processes, **1**, 45-55 (1992).
14. V. G. Sevastyanenko, L. Gu, and J. A. Bakken, Radiative Gas-Dynamics in Multicomponent Plasma, Int. Sem. Heat Mass Transfer under Plasma Cond., Cesme, Turkey (1994).
15. V. G. Sevastyanenko, L. Gu, and J. A. Bekken, Calculation of Radiative Heat-Transfer in Low-Temperature Plasmas, ISPC-12, Minneapolis, USA (1995).
16. B. Bowman, Properties of arcs in DC furnaces, 52nd Electric Furnace Conf., Nashville, USA (1994).

17. K. Ragaller, U. Kogelschatz, and W. R. Schneider, Z. Naturforschung, **28a**, 1321-1328 (1973).
18. K. C. Hsu and E. Pfender, J. Appl. Phys., **54**, 3818-3823 (1983).
19. C. Delalondre and O. Simonin, Modelling of high intensity arcs including a non-equilibrium description of the cathode sheath, Colloque de Physique, C5-1990, Supplement au J. de Physique, FASC. 18, 199-206 (1990).
20. P. Zhu, J. J. Lowke, and R. Morrow, J. Phys. D: Appl. Phys., **25**, 1221-1230 (1992).
21. J. J. Lowke, P. Kovitya, and H. P. Schmidt, J. Phys. D: Appl. Phys., **25**, 1600-1606 (1992).
22. A. Kaddani, C. Delalondre, O. Simonin, and H. Minoo, Thermal and Electrical Coupling of Arc Electrodes, TPP-3, Aschen, Germany (1994).
23. A. Kaddani, O. Simonin, and C. Delalondre, Numerical Investigations of the Cathode Region of Electric Arcs, ISPC-12, Minneapolis, USA (1995).
24. J. J. Lowke, R. Morrow, and J. A. Haidar, A Simplified Unified Theory of Arcs and Their Electrodes, ISPC-12, Minneapolis, USA (1995).
25. M. S. Benilov and A. Marotta, Theory of thermal arc spots on electrodes, TPP-3, Aachen, Germany (1994).
26. M. S. Benilov and A. Marotta, Theory of Cathodic Part of High-Pressure Arc Discharges, ISPC-12, Minneapolis, USA (1995).